Available online at www.sciencedirect.com
SCIENCE DIRECT®
Journal of Power Sources 144 (2005) 94–106
JOURNAL OF POWER SOURCES
www.elsevier.com/locate/jpowsour

Flow distribution and pressure drop in parallel-channel configurations of planar fuel cells

S. Maharudrayya, S. Jayanti *, A.P. Deshpande

Department of Chemical Engineering, IIT Madras, Chennai 600 036, India

Received 30 August 2004; received in revised form 2 December 2004; accepted 15 December 2004
Available online 15 February 2005

Abstract

Parallel-channel configurations for gas-distributor plates of planar fuel cells reduce the pressure drop, but give rise to the problem of severe flow maldistribution wherein some of the channels may be starved of the reactants. This study presents an analysis of the flow distribution through parallel-channel configurations. One-dimensional models based on mass and momentum balance equations in the inlet and exhaust gas headers are developed for Z- and U-type parallel-channel configurations. The resulting coupled ordinary differential equations are solved analytically to obtain closed-form solutions for the flow distribution in the individual channels and for the pressure drop over the entire distributor plate. The models have been validated by comparing the results with those obtained from three-dimensional computational fluid dynamics (CFD) simulations. Application of the models to typical fuel-cell distributor plates shows that severe maldistribution of flow may arise in certain cases and that this can be avoided by careful choice of the dimensions of the headers and the channels.

Keywords: Planar fuel cells; Parallel channels; Laminar flow; Flow distribution; Computational fluid dynamics

1. Introduction

A planar architecture for the gas-distribution channels of fuel cells provides an effective approach to achieve high utilization of the electrochemically active area. There are many flow configurations of the distributor plates for the flow of reactants, namely parallel, serpentine, parallel serpentine and interdigitated channels. For small fuel cells, where the pressure drop is of the order of 0.5–1 bar [1], serpentine or interdigitated channels can be used. For larger fuel cells, however, it is not possible to use these channels as the pressure drop would be of the order of a few bars. One way of decreasing the pressure drop would be to increase the depth of the channels. This would increase the hydraulic diameter of the channel and would thereby decrease the pressure drop significantly. While increasing the depth does not change the utilization of the electrochemically active area, it would increase the plate thickness and therefore make the fuel-cell stack bulkier and more expensive to produce. Using a parallel-channel configuration, where the flow rate through each channel is significantly less, also has the effect of decreasing the pressure drop substantially. There is, however, a possibility that the flow distribution is non-uniform. Some channels may be starved of the reactants while some others may have them in excess. Since the reactant distribution manifolds of the anode and the cathode sides are hydrodynamically decoupled, severe maldistribution of the reactants could occur across the distributor plate unless the configurations are properly designed.

In theory, it is possible to have a uniform flow distribution in the parallel channels, for example, this can be achieved by having a very large header cross-sectional area compared with that of a channel. Unfortunately, this has the effect of decreasing the active geometrical area of the distributor plate. Indeed, as shown later in Section 4, it is very difficult to obtain uniform flow distribution practically in a typical fuel-cell distributor plate with a parallel-channel configuration. Several factors, such as the plate dimensions, the inlet and the exhaust header dimensions, channel dimensions, flow rate and the aspect ratio, influence the flow distribution in a parallel-channel network and the designer must decide how to configure a channel network such that the

* Corresponding author.
E-mail address: sjayanti@iitm.ac.in (S. Jayanti).

0378-7753/$ – see front matter © 2004 Elsevier B.V. All rights reserved.
doi:10.1016/j.jpowsour.2004.12.018

Nomenclature

A_c	cross-sectional area of channel
A_h	cross-sectional area of header
b_c	depth of the channel
b_h	depth of header
C_1	constant in Eq. (29)
C_2	constant in Eq. (29)
C_3	constant in Eq. (32)
C_4	constant in Eq. (32)
C_{t1}	turning loss factor at dividing junction of header
C_{t2}	turning loss factor at combining junction of header
D_c	hydraulic-diameter of channel
D_h	hydraulic-diameter of header
F_1	flow parameter index
F_2	flow parameter index
f	friction factor
H	overall loss coefficient in channel
i	channel number
K_1	dimensionless quantity in Eq. (15a)
K_2	dimensionless quantity in Eq. (15b)
K_{fric}	frictional loss factor
L_c	length of channel
L_h	length of header
m	constant
m'	constant
m'_c	relative mass flow rate
N	number of channels
n	constant
n'	contant
P_1	pressure in the inlet header
P_2	pressure in the exhaust header
P_h	perimeter of the header
V_1	velocity in the inlet header
V_2	velocity in the exhaust header
V_c	velocity in the channel header
x	cartesian coordinate

Greek letters

Δ	difference operator
μ	absolute viscosity
ρ	density
τ_w	wall shear stress

Superscript

$'$	all prime quantities are dimensionless variables

appropriate flow rates and flow uniformity can be maintained across the surfaces of the membrane-electrode assembly (MEA). This possibility has been neglected in the models of proton-exchange membrane (PEM) fuel cells [2–4]; here, studies are limited to one or two channels or the assumption of uniform flow has been made implicitly or explicitly.

Much of the earlier experimental and theoretical work [5–10] on flow distribution in manifolds has been done for turbulent flow conditions through pipes of circular cross-section for various industrial applications, such as heat exchangers, irrigation systems and other chemical-processing streams. By contrast, the literature on laminar flow through a parallel-channel manifold is rather limited. Recently, Kim et al. [11] studied, using computational fluid dynamics (CFD) simulations, the effect of header shape on the flow distribution under laminar flow conditions in an eight-channel configuration. Boersma and Sammes [12,13] devised a computational model for the prediction of cell-to-cell distribution in solid oxide fuel-cell stacks. Hirata et al. [14] used a CFD code to study the pressure losses at dividing and combining junctions at a T-junction in a molten carbonate fuel-cell stack. Kee et al. [15] developed a numerical, one-dimensional model for a Z-type parallel-channel configuration (see Fig. 1) in a gas-distributor plate that was claimed to be also applicable to a fuel-cell stack. Koh et al. [16] presented a resistance concept based model for the evaluation of the flow distribution among cells in a fuel-cell stack.

In recent years, a number of new channel configurations have been studied. Conventional flow fields used in PEM fuel cells [17,18] are combinations of U-type flow configurations. Interdigitated flow fields [17,18] can be viewed as dividing and combining flow headers with parallel channels without forming any manifold. Jung et al. [19] have used different flow fields, such as parallel serpentine, spiral, Z-type and discontinuous channels in a three-dimensional PEMFC model, which has been solved with a CFD code. They showed that Z-type parallel channels offered the lowest pressure drop compared with the other three flow configurations but that the flow distribution in Z-type parallel channels was non-uniform. Hu et al. [18] showed that, for PEMFCs cells at low current density, both conventional and interdigitated flow fields was performed well, but that the pressure drop in interdigitated flow field was significantly higher than that in a conventional flow type.

The present study is motivated by the need to have a simple, ready-to-use hydrodynamic model for the calculation of flow rate and pressure drop in a parallel-channel configuration on a gas-distributor plate. Given the small size of these channels, experimental studies are difficult. In view of this, a model based on an adaptation of the analysis of Bassiouny and Martin [9,10] has been developed for Z- and U-type configurations of parallel channels on a gas-distributor plate. The unique feature of this model is that an analytical solution is possible with the result that explicit, closed-form expressions can be obtained to predict the relevant features. The accuracy of the model has been validated by comparison with the numerical results of Kee et al. [15] and with results obtained from CFD simulations for selected cases. Details of the model and its application to typical fuel-cell situations are described below.

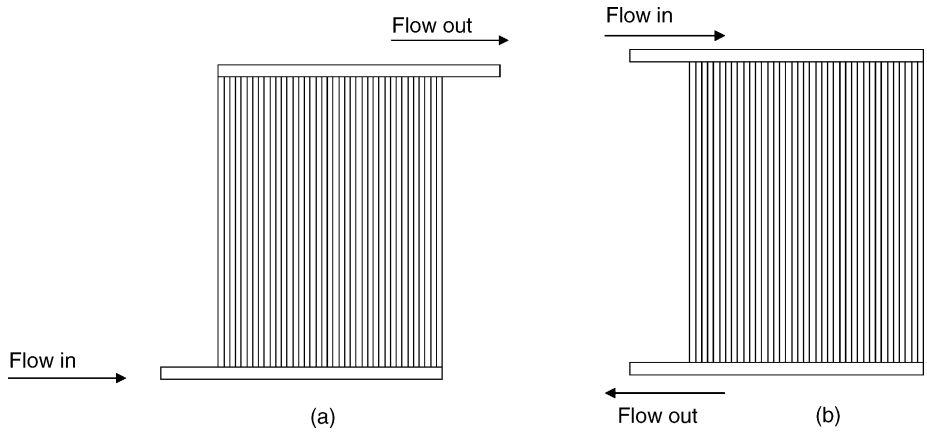

Fig. 1. Schematic diagram of (a) Z-type and (b) U-type parallel-channel flow configurations.

2. Problem formulation

Two types of parallel-channel configurations are considered, namely the Z-type and the U-type. These are shown schematically in Fig. 1(a and b), respectively. Each configuration has an inlet header (also called a dividing header) and an exhaust header (also called a combining header) to which a number of parallel channels of identical dimensions, namely width, depth and length, are connected. In a Z-type configuration, the inlet to the assembly is near the first channel and the outlet is near the last channel. In a U-type configuration, both the inlet and the outlet of the assembly are connected near the first channel. Other configurations are obviously possible, but attention here is restricted to these two.

The objective of the study is to predict, for a given flow rate to the inlet header, the flow rate through each of the parallel channels and the overall pressure drop between the inlet and the outlet of the assembly. To this end, one-dimensional mass and the momentum balance equations are written for the inlet and the exhaust headers and the channel flow-rate equations are derived. The approach is similar to that of Bassiouny and Martin [9,10] for turbulent flow through Z- and U-type manifolds. The major difference is that some of the assumptions made by these authors are not applicable for laminar flow. Therefore, a new set of assumptions is made to derive the corresponding expressions. The details are discussed below.

2.1. Z-type configuration

The mass balances and momentum balances on the control volume (CV) may be written differential equation form as derived by Bassiouny and Martin [9,10]. Consider a section of length Δx in the inlet header that encompasses the side channel through which part of the fluid enters from the left (Fig. 1). If $V(x)$, $P(x)$ are the velocity and pressure at location x and if V_c is the average velocity through the side channel, then, following Bassiouny and Martin [9,10], the continuity and momentum balance equations for this control volume can be written as follows:

mass balance:

$$\rho A_h V_1 = \rho A_h \left(V_1 + \frac{dV_1}{dx_1} \cdot \Delta x_1 \right) + \rho A_c V_c \tag{1}$$

where A_h and A_c are the cross-sectional areas of the header and the channel, respectively, V_1 the velocity at the inlet to the control volume and V_c is the velocity in the side channel. Setting $\Delta x = N/L_1$, where N is the number of parallel channels and L_1 is the length of the inlet header, Eq. (1) can be simplified as:

$$A_h \frac{dV_1}{dx_1} = -\frac{N}{L_1} V_c A_c \tag{2}$$

The momentum balance equation for the control volume in Fig. 2(a) can be written as

$$P_1 A_h - \left(P_1 + \frac{dP_1}{dx_1} \cdot \Delta x_1 \right) A_h - \tau_w P_h \Delta x_1 = \rho A_h \left(V_1 + \frac{dV_1}{dx_1} \cdot \Delta x_1 \right)^2 - \rho A_h {V_1}^2 + \rho A_c V_c V_{1c} \tag{3}$$

Here P_1 is the pressure at inlet to the CV, P_c the pressure at the side channel, τ_w the wall shear stress, V_{lc} the component of the velocity at the channel entrance in the inlet header direction and $P_h = 2(W_h + b_h)$ is the perimeter of the header. Writing $\tau_w = (f\rho V_1^2)/2$, where f is the friction factor for the wall shear stress and simplifying, the momentum balance equation becomes:

$$\frac{d}{dx_1}(\rho V_1 V_1) = -\frac{dP_1}{dx_1} - \frac{P_h f \rho V_1^2}{2A_h} - \frac{\rho A_c N}{A_h L_1} V_c V_{1c} \tag{4}$$

Bassiouny and Martin [9,10] neglected the frictional term compared with the inertial term (last term) in the above equation in their treatment of turbulent flow. In the present case of laminar flow, we retain the frictional term and neglect the inertial term to write the inlet header momentum equation as:

$$\frac{d}{dx_1}(\rho V_1 V_1) = -\frac{dP_1}{dx_1} - \frac{P_h f \rho V_1^2}{2A_h} \tag{5}$$

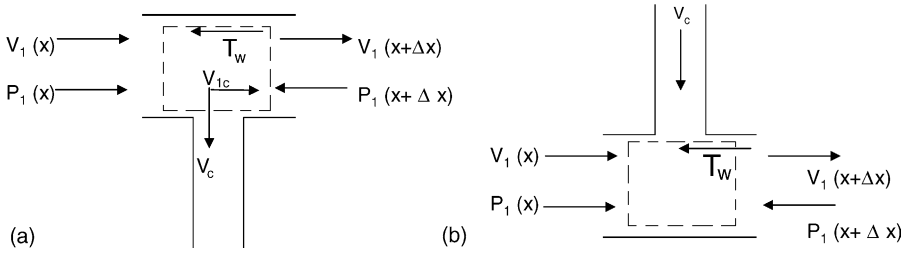

Fig. 2. Control volume in (a) inlet header and (b) exhaust header.

A similar analysis can be undertaken for the exhaust header. Considering a suitable control volume located in the outlet header (see Fig. 2(b)), the mass and momentum balance equations can be written, using similar simplifications, as follows:

- mass balance:

$$A_h \frac{dV_2}{dx_2} = \frac{N}{L_2} V_c A_c \tag{6}$$

- momentum balance:

$$\frac{d}{dx_2}(\rho V_2 V_2) = -\frac{dP_2}{dx_2} - \frac{P_h f \rho V_2^2}{2A_h} \tag{7}$$

Now, the flow rate through the channel is governed by the pressure difference between the inlet and the outlet of the channel, which is roughly the same as that between the inlet and the outlet headers at that channel. The velocity in the channel, V_c, is thus related to the pressure difference between the inlet and the outlet headers, $P_1 - P_2$, as according to:

$$P_1 - P_2 = \Delta P_{12} = H \tfrac{1}{2} \rho V_c^2 \tag{8}$$

where H is overall loss coefficient in the channel given by:

$$H = C_{t1} + C_{t2} + K_{fric} \tag{9}$$

where C_{t1} and C_{t2} are the turning loss factors for dividing and combining flow at the junctions (which are given empirically by Blevins [20], among others) and K_{fric} is the frictional loss coefficient, which for a straight pipe can be written as:

$$K_{fric} = \frac{4 f L_c}{D_c} \tag{10}$$

Here L_c is the channel length, D_c its hydraulic diameter $D_c = \frac{4 W_c b_c}{2(W_c + b_c)}$, where W_c and b_c are the width and the depth of the channel, respectively, and f is the friction factor given, for example, by the empirical correlation of Kays and Crawford [21]:

$$Re\, f = 13.84 + 10.38 \exp\left(\frac{-3.4}{a}\right) \tag{11}$$

where a is the channel aspect ratio $a = W_c/b_c$. For typical parallel-channel configurations, the dividing and the combining loss coefficients can be neglected in comparison with the straight pipe friction losses because of the low Reynolds number and the high length to diameter ratio of the channel ($L_c/D_c > 100$). Eq. (8) then reduces to

$$V_c = \Delta P_{12} \left(\frac{D_c^2}{2\mu L_c (Re\, f)_c} \right) \tag{12}$$

Assuming that the inlet and exhaust header lengths are of same length ($L_1 = L_2 = L_h$) and substituting this and non-dimensionalizing the lengths, velocities and pressures as:

$$x' = \frac{x}{L_h}, \qquad V' = \frac{V}{V_{in}}, \qquad P' = \frac{P}{\rho V_{in}^2}, \tag{13}$$

gives rise to the following coupled set of ordinary differential equations for the two velocities and the two pressures:

$$\frac{dV_1'}{dx'} = -K_1 \Delta P_{12}' \tag{14a}$$

$$\frac{dV_2'}{dx'} = +K_1 \Delta P_{12}' \tag{14b}$$

$$2V_1' \frac{dV_1'}{dx'} + \frac{dP_1'}{dx'} + K_2 V_1' = 0 \tag{14c}$$

$$2V_2' \frac{dV_2'}{dx'} + \frac{dP_2'}{dx'} + K_2 V_2' = 0 \tag{14d}$$

where K_1 and K_2 are given by

$$K_1 = \left(\frac{N_h A_c \rho V_{in}}{A_h} \right) \frac{D_c^2}{(Re\, f)_c 2 L_c \mu} \tag{15a}$$

$$K_2 = \left(\frac{P_h \mu (Re\, f)_h L_h}{2 A_h D_h \rho V_{in}} \right) \tag{15b}$$

2.2. U-type configuration

The analysis for the U-type configuration (see Fig. 1(b)) is similar to that for the Z-type counterpart. The control volumes in the inlet and exhaust headers remain the same as in Fig. 2. The mass and momentum balance equations for these control volumes, neglecting the inertial terms, can be written as follows:

- mass balance for the inlet header:

$$A_h \frac{dV_1}{dx_1} = -\frac{N}{L_1} V_c A_c \tag{16}$$

- momentum balance for the inlet header:

$$\frac{\mathrm{d}}{\mathrm{d}x_1}(\rho V_1 V_1) = -\frac{\mathrm{d}P_1}{\mathrm{d}x_1} - \frac{P_\mathrm{h} f \rho V_1^2}{2A_\mathrm{h}} \tag{17}$$

- mass balance for the exhaust header:

$$A_\mathrm{h}\frac{\mathrm{d}V_2}{\mathrm{d}x_2} = -\frac{N}{L_2} V_\mathrm{c} A_\mathrm{c} \tag{18}$$

- momentum balance for the exhaust header:

$$\frac{\mathrm{d}}{\mathrm{d}x_2}(\rho V_2 V_2) = -\frac{\mathrm{d}P_2}{\mathrm{d}x_2} + \frac{P_\mathrm{h} f \rho V_2^2}{2A_\mathrm{h}} \tag{19}$$

Comparing these with the corresponding ones for the Z-type configuration, it is found that the balance equations for the inlet header remain the same while those for the exhaust header are modified to take account of the fact that the flow rate for a U-type configuration, decreases with increasing x-direction in the exhaust header.

Rearranging and non-dimensionalizing as before, yields the following set of dimensionless equations for the U-type configuration:

$$\frac{\mathrm{d}V_1'}{\mathrm{d}x'} = -K_1 \Delta P_{12}' \tag{20a}$$

$$\frac{\mathrm{d}V_2'}{\mathrm{d}x'} = -K_1 \Delta P_{12}' \tag{20b}$$

$$2V_1'\frac{\mathrm{d}V_1'}{\mathrm{d}x'} + \frac{\mathrm{d}P_1'}{\mathrm{d}x'} + K_2 V_1' = 0 \tag{20c}$$

$$2V_2'\frac{\mathrm{d}V_2'}{\mathrm{d}x'} + \frac{\mathrm{d}P_i'}{\mathrm{d}x'} - K_2 V_2' = 0 \tag{20d}$$

where K_1 and K_2 are defined as in Eq. (15).

It is noted that Kee et al. [15] obtained the same set of relations as given in Eq. (14) for the Z-type configuration; the U-type configuration was not considered. The authors sought a numerical solution for these equations. We show here that an analytical solution is indeed possible.

3. Analytical solution and validation

An analytical solution for the governing equations of the Z- and U-type configurations is possible with further manipulation Eqs. (14) and (20), respectively. Noting that the sum of the inlet and the exhaust header velocity at any given section in the manifold is equal to average velocity at the inlet boundary yields:

$$V_1' + V_2' = 1 \tag{21}$$

Subtracting Eq. (14d) from Eq. (14c) and using Eq. (21) to eliminate one of the velocities, gives:

$$2\frac{\mathrm{d}V_1'}{\mathrm{d}x'} + \frac{\mathrm{d}(\Delta P_{12}')}{\mathrm{d}x'} + K_2(2V_1' - 1) = 0 \tag{22}$$

Using Eq. (14a) to eliminate ΔP_{12}, the following second-order ordinary differential equation for the Z-type configuration can be obtained:

$$\frac{\mathrm{d}^2 V_1'}{\mathrm{d}x'^2} - 2K_1\frac{\mathrm{d}V_1'}{\mathrm{d}x'} - 2K_1K_2V_1' + K_1K_2 = 0 \tag{23}$$

For the U-type configuration, the manifold continuity equation is given by:

$$V_1' = V_2' \tag{24}$$

and this leads to the following second-order equation for this configuration:

$$\frac{\mathrm{d}^2 V_1'}{\mathrm{d}x'^2} - 2K_1K_2V_1' = 0 \tag{25}$$

The flow distribution through the Z- and the U-type manifolds is governed, respectively, by Eqs. (23) and (25). These are second-order equations for which the boundary conditions can be written as follows:

$$\text{at inlet to the inlet header, i.e., at } x' = 0,\ V_1' = 1; \tag{26a}$$

$$\text{at the dead-end of the inlet header, i.e., at } x' = 1,\ V_1' = 0. \tag{26b}$$

3.1. Solution for Z-type configuration

The general solution for a velocity distribution equation is:

$$V_1'(x') = \text{complementary function (CF)} + \text{particular integral (PI)} \tag{27a}$$

For the Z-type configuration (Eq. (23)), the components can be written as

$$\mathrm{CF} = C_1\ \exp(mx') + C_2\ \exp(nx') \tag{27b}$$

$$\mathrm{PI} = \frac{K_1K_2}{2K_1K_2} = 0.5 \tag{27c}$$

where m and n are functions of K_1 and K_2:

$$m = K_1 + \sqrt{K_1^2 + 2K_1K_2},$$

$$n = K_1 - \sqrt{K_1^2 + 2K_1K_2} \tag{27d}$$

The constants C_1 and C_2 have to be determined from the boundary conditions; substituting these in Eq. (27b) gives:

$$C_1 = \frac{0.5(1+\exp(n))}{\exp(n) - \exp(m)}, \qquad C_2 = \frac{0.5(1+\exp(m))}{\exp(m) - \exp(n)} \tag{28}$$

Once the velocity in the inlet header is known, the velocity in the outlet header can be obtained from the manifold continuity equation, i.e., Eq. (22). The pressure drop in the channel can be obtained from Eq. (14a). Thus the pressure variation in the inlet and the outlet headers can be determined. In terms of

dimensionless quantities, these can be written for the Z-type configuration, as follows:

- relative mass flow rate through the channel, $m'_c (m'_c = V'_c A_h / A_c)$:

$$m'_c = -\frac{C_1 m \exp(mx') + C_2 n \exp(nx')}{N} \tag{29a}$$

- channel pressure drop:

$$\Delta P'_{12} = \frac{-(C_1 m \exp(mx') + C_2 n \exp(nx'))}{K_1} \tag{29b}$$

- pressure variation in inlet header:

$$P'_1 = P'_{1in} - \Big\{ C_1^2(\exp(2mx') - 1) + C_2^2(\exp(2nx') - 1) + 4C_1C_2(\exp((m+n)x') - 1) + \frac{(K_1C_1 + C_1m)}{m} \times (\exp(mx') - 1) + \frac{(K_2C_2 + C_2n)}{n} \times (\exp(nx') - 1) + 0.5K_2x' \Big\} \tag{29c}$$

where P'_{1in} is the pressure at the manifold inlet.

- pressure variation in outlet header:

$$P'_2 = P'_1 - \Delta P'_{12} \tag{29d}$$

- pressure drop in manifold:

$$\Delta P'_t = P'_1(0) - P'_2(1)$$

$$\Delta P'_t = C_1^2(\exp(2m) - 1) + C_2^2(\exp(2n) - 1) + 4C_1C_2(\exp(m+n) - 1) + \frac{K_1C_1 + C_1m}{m} \times (\exp(m) - 1) + \frac{K_2C_2 + C_2n}{n}(\exp(n) - 1) + 0.5K_2 + \frac{C_1m \exp(m) + C_2n \exp(n)}{K_1} \tag{29e}$$

3.2. Solution for U-type configuration

The complementary function and the particular integral for this case, i.e., Eq. (25) and boundary conditions given by Eq. (26) are

$$\mathrm{CF} = C_3 \exp(m'x') + C_4 \exp(n'x') \tag{30a}$$

$$\mathrm{PI} = 0 \tag{30b}$$

where

$$m' = -n' = \sqrt{2K_1K_2} \tag{30c}$$

Substitution of boundary conditions yields the values of C_3 and C_4 as:

$$C_3 = \frac{-\exp(n')}{\exp(m') - \exp(n)}, \qquad C_4 = \frac{\exp(m')}{\exp(m') - \exp(n')} \tag{31}$$

The variation of the flow rate in the channels and the pressure variations in the headers can now be found. In terms of dimensionless quantities, these can be written for the U-type configuration, as follows:

- relative mass flow rate through the channel, $m'_c (m'_c = V'_c A_h / A_c)$:

$$m'_c = -\frac{C_3 m' \exp(m'x') + C_4 n' \exp(n'x')}{N} \tag{32a}$$

- channel pressure drop:

$$\Delta P'_{12} = \frac{-(C_3 m' \exp(m'x') + C_4 n' \exp(n'x'))}{K_1} \tag{32b}$$

- pressure variation in the inlet header:

$$P'_1 = P'_{1in} - \Big\{ C_3^2(\exp(2m'x') - 1) + C_4^2(\exp(2n'x') - 1) + 2C_3C_4(\exp((m'+n')x') - 1) + \frac{K_2C_3}{m'}(\exp(m'x') - 1) + \frac{K_2C_4}{n'}(\exp(n'x') - 1) \Big\} \tag{32c}$$

where P_{1in} is the pressure at the manifold inlet.

- pressure variation in exhaust header:

$$P'_2 = P'_1 - \Delta P'_{12} \tag{32d}$$

- pressure drop in manifold:

$$\Delta P'_t = P'_1(0) - P'_2(0) = \Delta P'_{12}(0)$$

$$\Delta P'_t = -\frac{C_3m' + C_4n'}{K_1} \tag{32e}$$

3.3. Flow distribution maps

The flow distribution among the parallel channels can now be examined with the help of Eqs. (29a) and (32a) for Z- and U-type configurations, respectively. Examination of these equations shows that the relative flow-rate distribution among the channels is influenced by the parameters K_1 and K_2. Kee et al. [15] generated a flow distribution "map" based on the numerical solution of Eq. (14) for the Z-type configuration. Similar maps obtained from the present analytical solution for the Z- and the U-types of configuration are shown in Fig. 3. Here, contours of the parameter F_1 are defined as

$$F_1 = \frac{m'_{c,max} - m'_{c,min}}{m'_{c,max}} \tag{33}$$

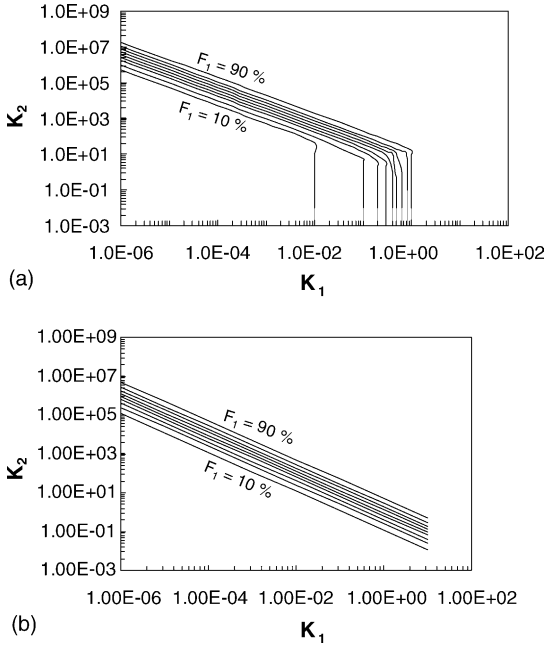

Fig. 3. Flow distribution contour maps for (a) Z-type and (b) U-type configurations.

where $m'_{c,max}$ and $m'_{c,min}$ are the maximum and minimum flow rates in a set of parallel channels and are plotted as a function of K_1 and K_2. The value of F_1 varies between 0 and 1 and indicates the extent of non-uniformity of the flow distribution among channels. If $F_1 = 0$, all channels have the same flow rate, while $F_1 = 1$ indicates that one (or more) of the channels have zero flow rate. The lowermost contour is for $F_1 = 0.1$ and the uppermost is for $F_1 = 0.9$; others vary for F_1 between 0.1 and 0.9 with an increment of 0.1. The region in Fig. 3 to the left of and below the contours indicates nearly uniform distribution, while the region to the right of and above the lines shows poor distribution. The data in Fig. 3(a) are identical to those produced by Kee et al. [15] from their numerical solution of the same set of relationship as Eq. (14). Comparing the flow maps for the Z- and the U-type configurations, it is found that although there are similarities, they are not identical and that it is possible to have uniform distribution with the U-type configuration at lower values of K_2 at a given K_1.

The flow rate distribution for a 20-channel case is shown in Fig. 4 for the Z- and the U-type configurations for four different combinations of K_1 and K_2. The results show that for some combinations of K_1 and K_2 (e.g., Fig. 4(a)), both configurations are equally good; for some other combination (e.g., Fig. 4(b)), the Z-type is patently better; for certain other combinations (e.g, Fig. 4(c)), the U-type is better and finally, for some other combinations of K_1 and K_2 (e.g., Fig. 4(d)), both configurations are equally bad as far as flow uniformity is concerned. The pressure distributions in the inlet and exhaust headers for these arrangements are shown in Fig. 5. These show that the pressure may remain practically unchanged, decrease or increase along the length of the header. If the pressure difference across the headers is constant, a nearly uniform flow results; otherwise (e.g., Fig. 5(d)) severe non-uniformity of flow may occur.

In addition to the flow distribution parameter F_1 which is based on the maximum and minimum values of the flow rates, the root mean square (rms) value of the deviation from the mean flow rate, F_2, defined as:

$$F_2 = \frac{\sqrt{\sum_{i=1}^{n} \left(m'^{i}_{c} - \overline{m'_c}\right)^2}}{N\overline{m'_c}} \tag{34}$$

also characterizes the relative flow split. The two parameters, F_1 and F_2, are listed in Table 1 for various cases including the four discussed above. Both the parameters can be used to define acceptable levels of flow uniformity for practical applications.

3.4. Validation

The accuracy of the present solution, which exhibits the complicated parametric dependence shown in Figs. 4 and 5, is verified in two independent ways, as follows:

- By comparison of the results of the Z-type configuration with the numerical solution of Kee et al. [15] who solved the same set of equations. The flow pattern map for

Table 1
Effect of K_1 and K_2 on flow distribution

K_1	K_2	Z-type			U-type		
		F_1	F_2	$\Delta P'_{total}$	F_1	F_2	$\Delta P'_{total}$
1.0E − 04	1.0E − 02	3.6E − 05	5.8E − 05	1.0E + 04	3.6E − 05	2.8E − 07	1.0E + 04
1.0E − 04	1.0E + 01	3.6E − 05	1.0E − 04	1.0E + 04	3.6E − 05	2.8E − 04	1.0E + 04
1.0E − 04	1.0E + 02	3.6E − 05	7.7E − 04	1.0E + 04	7.5E − 03	2.5E − 03	1.0E + 04
1.0E − 02	1.0E − 02	1.9E − 02	5.8E − 03	6.8E + 01	8.0E − 05	2.8E − 05	1.0E + 02
1.0E − 02	1.0E + 01	3.9E − 02	1.0E − 02	1.1E + 02	8.5E − 02	2.8E − 02	1.1E + 02
1.0E − 02	1.0E + 02	2.1E − 01	7.3E − 02	1.7E + 02	5.1E − 01	2.4E − 01	1.6E + 02
1.0E + 00	1.0E − 02	8.5E − 01	5.9E − 01	3.5E − 02	7.4E − 03	2.8E − 03	1.0E + 00
1.0E + 00	1.0E + 01	7.9E − 01	6.3E − 01	7.4E + 00	9.7E − 01	9.9E − 01	4.5E + 00
1.0E + 00	1.0E + 02	1.0E + 00	1.8E + 00	5.7E + 01	1.0E + 00	1.7E + 00	1.4E + 01

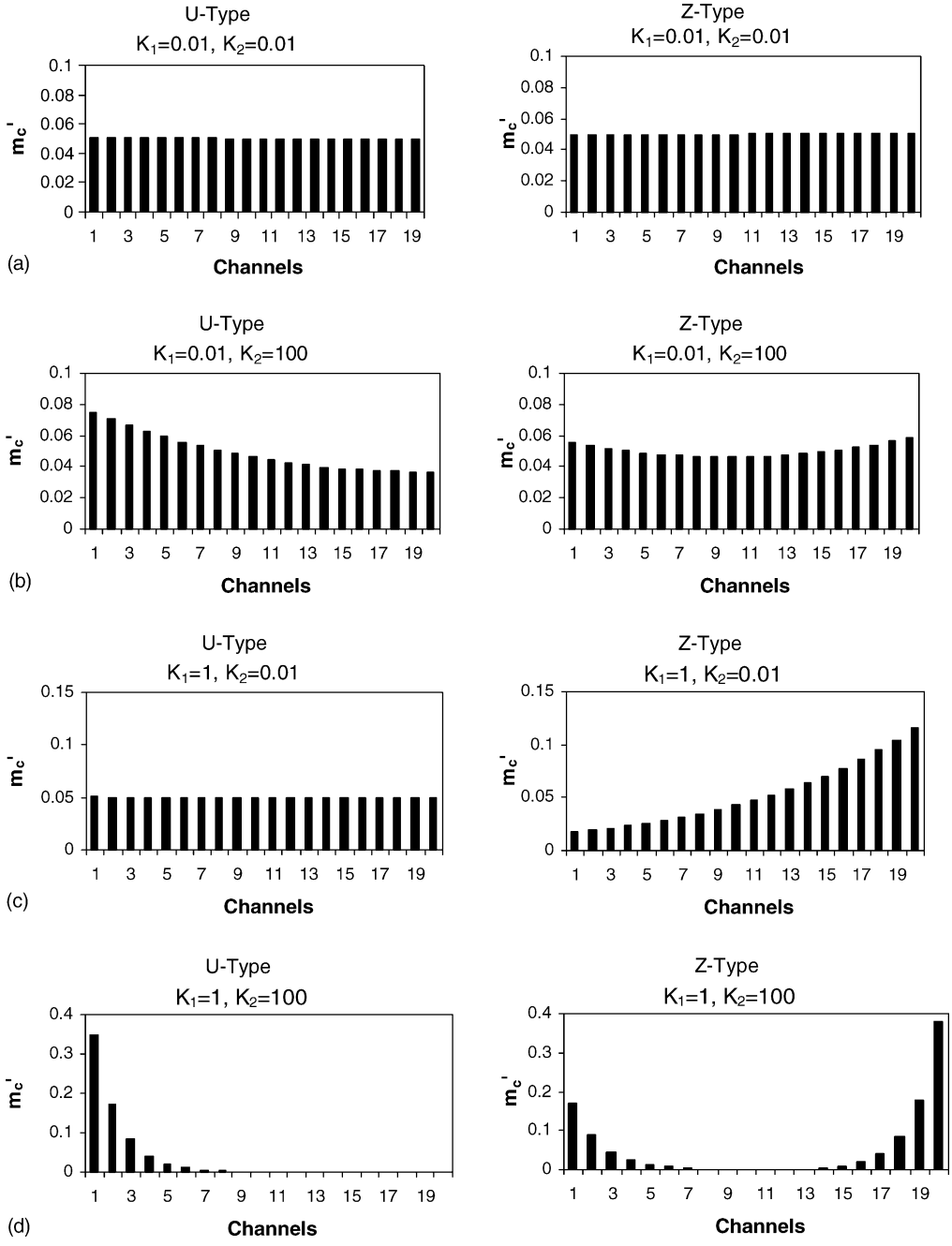

Fig. 4. Relative mass flow rate distribution for 20 channels at different K_1 and K_2 values.

this configuration obtained from the present analytical solution (Eq. (28) and Fig. 3(a)) is identical to that given by Kee et al. [15]. Since both solve the same equations, this shows that the analytical solution for the Z-type configuration is correct.

- A second and more reliable source of confirmation of accuracy comes from three-dimensional CFD simulations carried out for specific cases as part of the present study. Here, laminar flow through 10- and 20-parallel channels in Z- and U-type configurations has been simulated for different Reynolds numbers using the commercial CFD code CFX developed by AEA Technology, UK. CFX has been previously been used by the present authors [1] to study pressure losses in serpentine channels and the same methodology of calculation is used in the present case for parallel channels of configurations shown in Fig. 1. A comparison of the dimensionless (relative) mass flow rate obtained from the analytical and the CFD solutions for both flow configurations at a header Reynolds number of 650 is given in Fig. 6. There is good agreement between the analytical and the CFD solutions. The effect of Reynolds number on the relative flow distribution is shown in Fig. 7 for the Z- and U-

type configurations. Both the CFD and the analytical solutions are in good agreement and further indicate that as *Re* increases, the flow becomes non-uniform. By contrast, the relative flow distribution is independent of the Reynolds number for a U-type configuration; this fact is borne out well by both CFD and analytical solutions. Finally, the predicted pressure drop across the manifold by the CFD and the analytical solutions for a Z-type configuration are compared in Fig. 8 as a function of Reynolds number. This again shows excellent agreement. Given that no approximations are made in the momentum balance equations in the CFD solution, this good agreement shows that neglect-

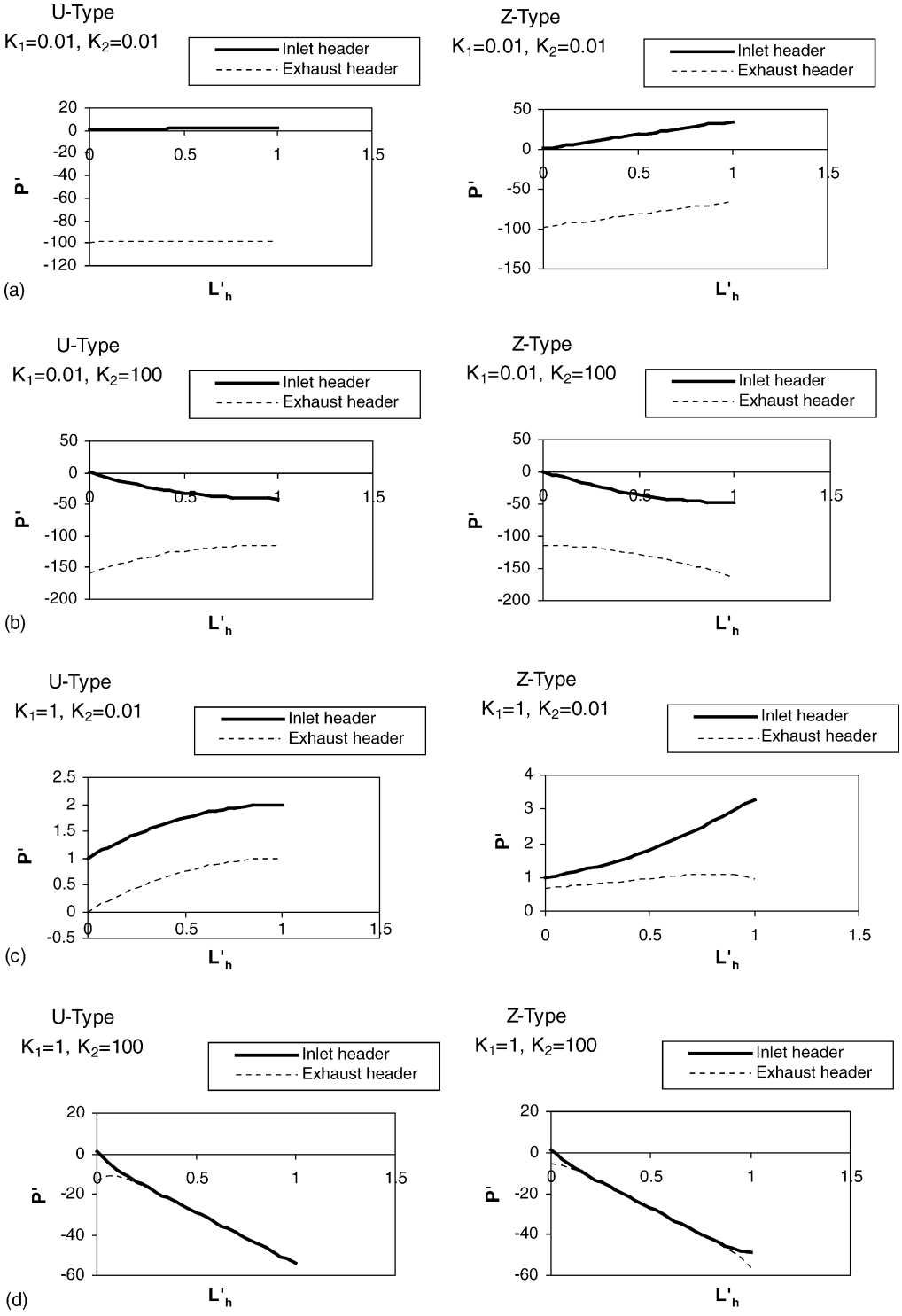

Fig. 5. Dimensionless pressure variation along dimensionless header length at different K_1 and K_2 values.

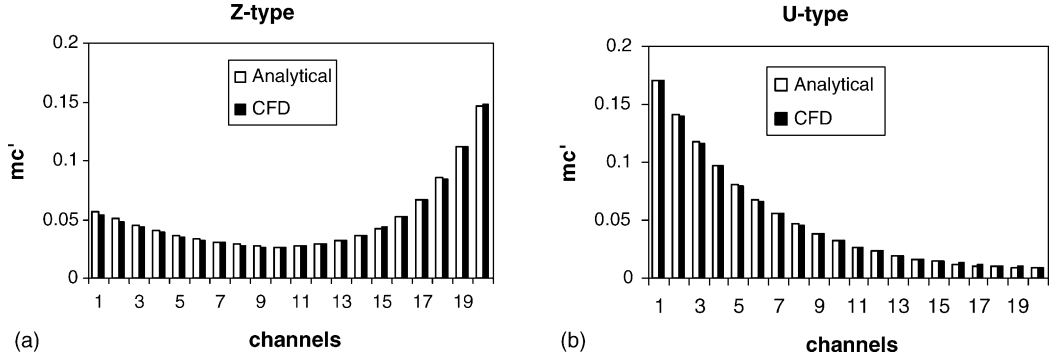

Fig. 6. Comparison of relative mass flow rate distribution obtained from analytical and CFD solutions for 20 channels in (a) Z-type and (b) U-type flow configurations.

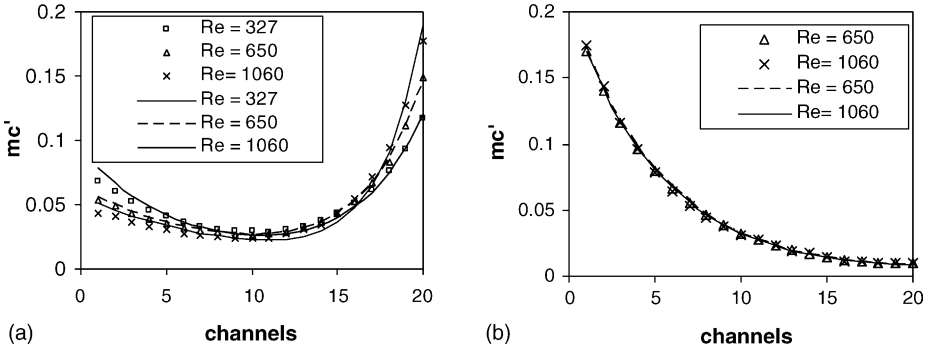

Fig. 7. Effect of Reynolds number (at inlet of inlet header) on flow distribution obtained from analytical (lines) and CFD (symbols) solutions in (a) Z-type and (b) U-type flow configurations.

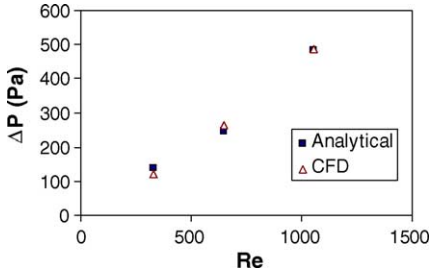

Fig. 8. Comparison of manifold pressure drop obtained from analytical and CFD solution for 20 channels in Z-type flow configuration.

ing the inertial term in the momentum balance equations is justified.

3.5. Algorithm for flow distribution calculation

The above comparisons with numerical and CFD solutions show that the present analytical approach is accurate. The steps leading to the calculation of the flow distribution and pressure drop in the manifold are summarized here in the form of an algorithm.

We denote (see Fig. 9) the width and the length of the polar plate by W_p and L_p, respectively. The terms W_c, L_c, W_h, L_h are the width and the length of the channel, and the width and

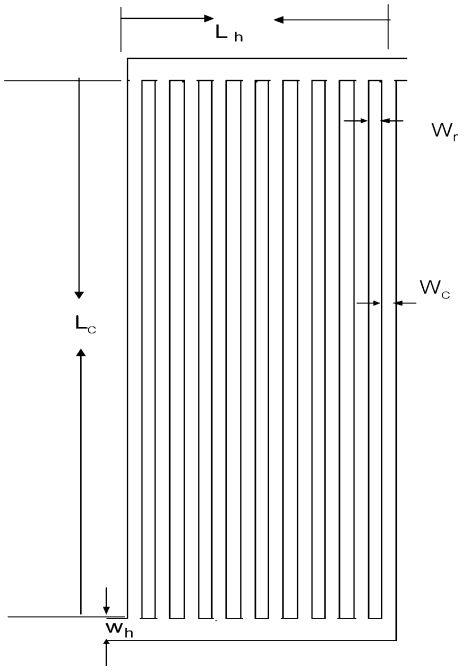

Fig. 9. Representation of dimensions in Z-type parallel-channel configuration.

length of the header, respectively. The active area of the plate is thus $L_h(L_c + 2W_h)$. The terms b_h and b_c, the depth of the header and depth of the channel, are not shown in Fig. 9. The rib width between the two channels is denoted as W_r. The number of channels (N) to be hewn out of the plate is given by:

$$L_h = NW_c + (N-1)W_r \text{ or } N = \frac{L_h + W_r}{W_c + W_r} \tag{35}$$

With this nomenclature, the algorithm can be written as follows:

Step 1. For a given active area and for a given parallel configuration (Z-type or U-type), fix W_r, W_h and W_c, L_h, D_h and D_c and evaluate A_h, A_c, N and L_c.

Step 2. Calculate the product of Reynolds number and friction factor for the header $(Re\,f)_n$ and the channel $(Re\,f)_c$ as a function of their aspect ratios using Eq. (11).

Step 3. From the volumetric flow rate and the header dimensions, calculate V_{in}, the velocity at the header inlet.

Step 4. Calculate K_1 and K_2 by Eqs. (15a) and (15b).

Step 5. Calculate the set of constants $\{m, n, C_1, C_2\}$ or (m', n', C_3, C_4) as appropriate using Eqs. (27c) and (28) for Z-type and Eqs. (30c) and (31) for the U-type configurations, respectively.

Step 6. Fix the number of points along the headers as the number of channels, N, calculate the flow rate distribution and pressure variation in the headers using Eqs. (29a), (29c) and (29d) for Z-type and Eqs. (32a), (32c) and (32d) for U-type, respectively.

Step 7. Calculate the flow uniformity indices F_1 and F_2 using Eqs. (33) and (34) and the pressure drop across the manifold using Eqs. (29e) and (32e). If the flow uniformity indices and the pressure drop across the manifold are not satisfactory, go back to Step 1 and try with different values for W_r, etc.

4. Application to fuel-cell stacks

We now consider the above results for a typical fuel-cell application. We start by rewriting the important flow distribution parameters K_1 and K_2 in terms of dimensionless groups as:

$$K_1 = K_{11}K_{12}K_{13}K_{14} = \left(\frac{NA_c}{A_h}\right)\left(\frac{\rho V_{in} D_c}{\mu}\right) \times \left(\frac{D_c}{2L_c}\right)\left(\frac{1}{(Re\,f)_c}\right) \tag{36}$$

$$K_2 = K_{21}K_{22}K_{23} = \left(\frac{\mu}{D_h \rho V_{in}}\right)\left(\frac{2L_h}{D_h}\right)(Re\,f)_h \tag{37}$$

K_1 has dimensionless groups such as ratio of the total cross-sectional area of the channels to that of the header, channel Reynolds number based inlet velocity at the header, channel length to diameter ratio, a constant $(Re\,f)_c$. For typical fuel-cell sizes, the area ratio (A_c/A_h) will be not be less than 0.25, and so the group K_{11} is of the order of 10. The group K_{12} (which is Re_c based on inlet velocity) will be of the order of 100. K_{13} will be of the order of about 0.01 and K_{14} will be around 0.05. Thus, for typical fuel-cell applications, K_1 is of the order of 0.5. Similarly, K_2 has dimensionless groups, such as header Reynolds number, based on inlet velocity at the inlet header, header length to diameter ratio, a constant $(Re\,f)_h$. For typical fuel-cell applications, K_{21}, K_{22} and K_{23} will be of the order of 0.001, 100 and 20, respectively. Thus, K_2 will be typically of the order of 2. Indeed, calculations

Table 2
Effect of header/channel dimensions on flow distribution and pressure drop

Header dimensions; width × depth (mm)	Channel dimensions; width × depth (mm)	K_1	K_2	Z-type			U-type		
				F_1	F_2	$\Delta P'_{total}$	F_1	F_2	$\Delta P'_{total}$
4 × 0.72	2 × 0.72	3.06	4.10	0.92	0.138	759.16	0.98	0.173	410.84
4 × 0.72	1.5 × 0.72	2.74	4.09	0.91	0.113	781.57	0.97	0.155	468.17
4 × 0.72	1 × 0.72	2.18	4.07	0.88	0.081	806.26	0.97	0.122	485.49
4 × 1.5	2 × 0.72	0.70	2.30	0.62	0.053	183.76	0.66	0.060	169.25
4 × 1.5	1.5 × 0.72	0.63	2.29	0.59	0.043	192.95	0.64	0.048	180.62
4 × 1.5	1 × 0.72	0.50	2.28	0.53	0.029	216.53	0.57	0.032	209.06
8 × 0.72	2 × 0.72	0.76	7.72	0.74	0.066	396.70	0.93	0.140	282.51
8 × 0.72	1.5 × 0.72	0.69	7.70	0.71	0.053	405.56	0.92	0.115	298.20
8 × 0.72	1 × 0.72	0.54	7.67	0.65	0.037	429.41	0.89	0.082	335.12
8 × 1.5	2 × 0.72	0.18	3.96	0.27	0.015	119.00	0.42	0.030	116.89
8 × 1.5	1.5 × 0.72	0.16	3.94	0.27	0.013	128.31	0.40	0.023	125.71
8 × 1.5	1 × 0.72	0.13	3.93	0.22	0.009	151.66	0.34	0.016	150.65
8 × 1.5	2 × 0.72	0.08	5.69	0.17	0.009	106.05	0.31	0.020	104.96
8 × 1.5	1.5 × 0.72	0.07	5.67	0.16	0.007	115.50	0.29	0.016	114.74
8 × 1.5	1 × 0.72	0.06	5.65	0.10	0.004	138.98	0.25	0.010	138.53

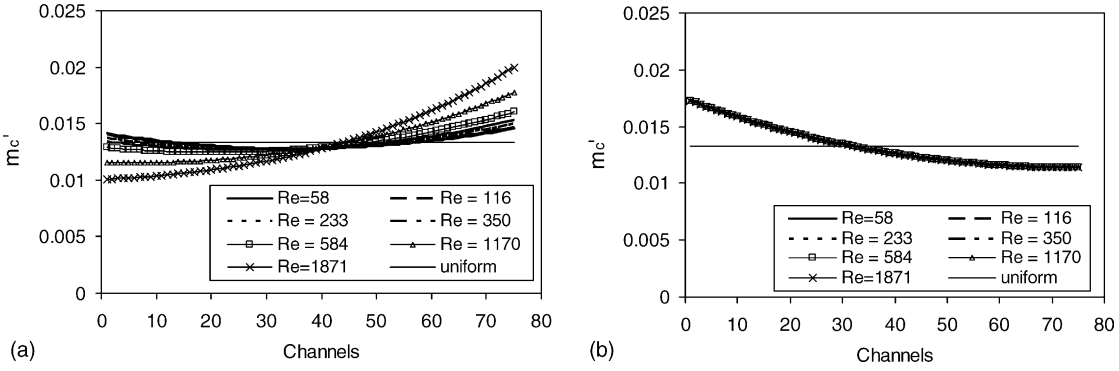

Fig. 10. Effect of Reynolds number on flow distribution of in (a) Z-type and (b) U-type flow configurations.

over a range of the parametric values (see Table 2) indicate that $0.05 < K_1 < 5$ and $1 < K_2 < 10$. Examination of the flow distribution maps (Fig. 3) shows that, in this range of K_1 and K_2, significant variations in the performance parameters are possible. We use the above calculation methodology as a basis to investigate what scope for optimization exists for a typical fuel cell.

To this end, flow distribution and pressure drop calculations have been done for a range of channel dimensions, header dimensions and flow rates for a fuel-cell distributor plate with an active area of 300 cm^2 (150 mm × 200 mm). The reference case is that of a parallel-channel configuration with a header width of 4 mm and depth of 0.72 mm, a channel width of 2 mm, depth of 0.72 mm and a rib width of 2 mm between channels. Variations of these geometric dimensions, which are within the scope of a designer, are considered for both Z- and U-type configurations and the results are discussed below.

4.1. Effect of header/channel aspect ratio on flow distribution

The effect of changing the dimensions of the header (width and depth), channel (width × depth) and rib width, which will have an effect on flow distribution and pressure drop is shown in Table 2, where the flow uniformity indices, F_1 and F_2, corresponding to each case are listed. It is to be recalled that the lower the values of F_1 and F_2, the better is the flow distribution through the parallel channels. The header width was varied from 4 to 12 mm, depth from 0.72 to 1.5 mm, channel width from 2 to 1 mm, rib width from 2 to 1 mm. For all the combination of header and channel dimensions, the mass flow rate was kept constant at 2.08×10^{-5} kg^{-1} s. By keeping the header dimensions constant, by decreasing the channel width and also rib width, the number of parallel channels will increase from 38 to 75 approximately. One would expect a decrease in pressure drop as the number of channels increases but in this case the channel hydraulic diameter decreases as the number of channels increases so the pressure drop increases. The flow distribution parameters increase with increase in the number of channels. From the data in Table 2, it is clear that for the header dimension of 12 mm width and 1.5 mm depth, the flow distribution is nearly uniform. This shows that to have uniform flow distribution, it is necessary to have very large header dimensions compared with channel dimensions. If the header dimension is increased, the land area (i.e., non-active area for the flow) will decrease near the header and this may increase the resistance in collecting the current as the bipolar plates also act also as current-collectors. The dimensions of the header and the channels and also the land area for the current-collectors can be optimized.

It is observed for all the Z-type flow configurations illustrated above, a minimum exists in the flow distributions. The minimum flow rate was found to be almost in the central channel (e.g., 38–75 channels). By contrast, the U-type configuration always shows a monotonic variation in the flow rate. These results can be confirmed analytically.

4.2. Effect of flow rate on flow distribution

Flow distribution calculations were undertaken for a wide range of mass flow rates that are typically used in fuel-cell stacks. The calculations are based on a header width of 8 mm and depth of 1.5 mm, a channel width of 1 mm, a depth of 0.72 mm and a rib width of 1 mm. Flow distribution curves are plotted against the number of channels for various flow rates in Fig. 10. It is seen that the non-uniformity in the flow distribution increases with increase in flow distribution for the Z-type flow configuration. It is found that, in this configuration, the last channel always receives the highest mass flow. The minimum flow rate channel lies near the centre, but it shifts towards the first channel as the Reynolds member increases. With the U-type configuration, the flow distribution is independent of flow rate and there is a monotonic variation in the flow rate from the first to the last for all the flow rates. It is noted that the U-type configuration gives better performance than the Z-type at high flow rates. The values of F_1 and F_2 and the pressure drop are tabulated in Table 2 for all flow rates. The pressure drop in the plate can also be seen in Table 3. The pressure drop varies linearly with flow rate.

Table 3
Effect of inlet flow rate on flow distribution (header 8 × 1.5 mm, channel 1 × 0.72 mm)

Flow rate (kg s^{-1})	Re_{hin}	K_1	K_2	Z-type			U-type		
				F_1	F_2	ΔP (Pa)	F_1	F_2	ΔP (Pa)
5.00E−06	58	0.01	39.30	0.11	4.27E	15.28	0.34	0.015	15.07
1.00E−05	116	0.03	19.65	0.13	4.51E	30.82	0.34	0.015	30.27
2.00E−05	235	0.05	9.83	0.15	5.30E	60.35	0.34	0.015	59.58
3.00E−05	467	0.08	6.55	0.17	6.36E	91.52	0.34	0.015	90.50
5.00E−05	584	0.13	3.93	0.22	8.90E	151.67	0.34	0.015	150.68
1.00E−04	1170	0.25	1.97	0.35	1.61E	297.25	0.34	0.015	301.72
1.60E−04	1870	0.40	1.23	0.50	2.50E	456.93	0.34	0.015	482.1

4.3. Effect of fuel-cell size

The calculations were repeated for two more fuel-cell plate sizes, namely, for a much smaller active are of 25 cm^2 (50 mm × 50 mm) and for a much larger active area of 750 cm^2 (250 mm × 300 mm). For all the sizes, a header width of 4 mm, depth of 0.72 mm, a channel width of 2 mm, depth of 0.72 and a rib width of 2 mm were used. The mass flow rate at the inlet boundary of the inlet header was kept at 4.17×10^{-5} kg s^{-1}. The increase in the size adversely affected the flow distribution due to increase in the number of channels from 26 to 150. The data in Section 4 showed that an increase in N will increase K_1, which will affect the flow distribution adversely. It can be recalled that one should have a larger header-to-channel ratio to attain uniform or near-uniform flow distribution. A large header for a small fuel cell is not possible, and one has to optimise the header and the channel dimensions carefully.

5. Conclusions

The pressure loss in a fuel-cell stack is one of the important determinants of overall fuel-cell efficiency, while uniform flow distribution over the entire plate is necessary to use optimally the entire active land area of the plate. In the present study, a one-dimensional analysis has been presented for the evaluation, in the form of a closed-form solution, of pressure drop and relative flow distribution in the parallel channels of Z- and U-type configurations. The models have been validated by comparison with results obtained from full three-dimensional CFD simulations.

The present analysis shows that for typical fuel-cell distributor plate dimensions, mild to severe flow maldistribution is possible for both Z- and U-type configurations. The severity of maldistribution depends strongly on the geometric factors of the parallel-channel configuration such as the channel dimensions, the header dimensions and the rib width between the parallel channels. It is shown that by adjusting these, a nearly uniform flow distribution can be achieved.

The proposed model is valid only for laminar flows, which is the case with most parallel-channel configurations. Although it has been developed specifically for Z- and U-type configurations, it can be extended readily to combinations of these configurations, such as the discontinuous channel arrangement [19], double-U arrangement and interdigitated flow configurations [17,18]. This enables the designer to optimize the channel configuration to ensure near-uniform flow distribution while maintaining a low overall pressure drop across the distributor plate.

Acknowledgements

The work reported here has been carried out under a research grant from the Ministry of Non-conventional Energy Resources, India. The CFD computations have been carried out using the facilities of the CFD Centre, IIT Madras, India.

References

[1] S. Maharudrayya, S. Jayanti, A.P. Deshpande, J. Power Sources 138 (2004) 1–13.
[2] V. Garau, L. Hongtan, S. Kakac, AIChE J. 44 (1998) 2410–2422.
[3] S. Um, C.-Y. Wang, K.S. Chen, J. Electrochem. Soc. 147 (2000) 4485–4493.
[4] T. Berning, D.M. Lu, N. Djilali, J. Power Sources 106 (2002) 284–294.
[5] A. Acrivos, B.D. Babcock, R.L. Pigford, Chem. Eng. Sci. 10 (1959) 112–124.
[6] M. Pearlmutter, Basic J. Eng. Trans. ASME (1961) 361–370.
[7] R.A. Bajura, J. Power Eng. Trans. ASME (1971) 7–12.
[8] R.A. Bajura, E.H. Jones, J. Fluids Eng. Trans. ASME (1976) 654–666.
[9] M.K. Bassiouny, H. Martin, Chem. Eng. Sci. 39 (1984) 693–700.
[10] M.K. Bassiouny, H. Martin, Chem. Eng. Sci. 39 (1984) 701–704.
[11] S. Kim, E. Choi, Y.I. Cho, Int. Comm. Heat Mass Transfer 22 (1995) 329–341.
[12] R.J. Boersma, N.M. Sammes, J. Power Sources 63 (1996) 215–219.
[13] R.J. Boersma, N.M. Sammes, J. Power Sources 66 (1997) 41–45.
[14] H. Hirata, T. Nakagaki, M. Hori, J. Power Sources 102 (2001) 118–123.
[15] J.R. Kee, P. Korada, K. Walters, M. Pavol, J. Power Sources 109 (2002) 148–159.
[16] H.J. Koh, K.H. Seo, G.C. Lee, S.Y. Yoo, C.H. Lim, J. Power Sources 115 (2003) 54–65.
[17] T.V. Ngyen, J. Electrochem. Soc. 143 (1996) 2767–2772.
[18] G. Hu, J. Fan, S. Chen, Y. Liu, K. Cen, J. Power sources 136 (2004) 1–9.
[19] H.-M. Jung, W.-Y. Lee, J.-S. Park, C.-S. Kui, Int. J. Hydrogen Energy 29 (2004) 945–954.
[20] D. Robert Blevins, Applied Fluid Dynamics Handbook, Van Nostrand Reinhold Co. Inc., 1984.
[21] W.M. Kays, M.E. Crawford, Convective Heat and Mass Transfer, McGraw-Hill, New York, 1980.